Dalton Transactions

ROYAL SOCIETY OF CHEMISTRY

PAPER

View Article Online
View Journal | View Issue

Cite this: *Dalton Trans.*, 2023, **52**, 3699

Thermodynamic and voltammetric study on carnosine and ferrocenyl-carnosine†

Chiara Abate,[a] Anna Piperno,[a] Alex Fragoso,[b] Ottavia Giuffrè,[a] Antonino Mazzaglia,[c] Angela Scala[a] and Claudia Foti*[a]

Received 22nd December 2022,
Accepted 11th February 2023

DOI: 10.1039/d2dt04093j

rsc.li/dalton

A potentiometric study on the interactions of L-carnosine (CAR) (2-[(3-aminopropanoyl)amino]-3-(1*H*-imidazol-5-yl)propanoic acid) with two toxic metal cations, Hg^{2+} and Cd^{2+}, is reported here. The elucidation of the metal (M^{2+})–CAR interactions in aqueous solution highlighted the speciation model for each system, the dependence of the formation constants of the complex species on ionic strength ($0.15 \leq I$/mol $L^{-1} \leq 1$) and temperature ($288.15 \leq T/K \leq 310.15$) and changes in enthalpy and entropy. The sequestering ability of CAR towards the two metal ions was quantified and compared with that with Pb^{2+}, previously determined. Considering the complexing ability of CAR and its unclear electrochemical properties, a more electroactive derivative, the ferrocenyl-carnosine (FcCAR), was synthesized and its complexing ability was evaluated by UV-vis spectroscopy. FcCAR electrochemical properties were investigated by Cyclic Voltammetry (CV) and Differential Pulse Voltammetry (DPV) on Screen-Printed Electrodes (SPEs), to evaluate its sensing properties. Electrochemical responses in the presence of Hg^{2+} and Pb^{2+} have been shown to be promising for the electrochemical detection of these metal cations in aqueous environment.

Introduction

L-Carnosine (CAR) (2-[(3-aminopropanoyl)amino]-3-(1*H*-imidazol-5-yl)propanoic acid) (Fig. 1) is a naturally occurring dipeptide with a non-enzymatic free-radical scavenger activity.[1,2]

Although the specific biological role of CAR is not completely understood, many studies highlighted its extensive antioxidant potential as an effective quencher of intracellular reactive oxygen species (ROS) and reactive nitrogen species (RNS), as well as a scavenger of reactive carbonyl species (RCS).[3–10] The physiological behavior of CAR depends on its complexation of bivalent metal cations, *e.g.*, Cu^{2+}, Mn^{2+}, Zn^{2+}, Ru^{2+}, Co^{2+}, Ni^{2+}, Cd^{2+}, Mg^{2+}, and Ca^{2+}.[1] It is a polydentate ligand with five potential metal-coordinating sites, *i.e.*, two imidazole nitrogens, the carboxylate group, a peptide linkage and a terminal amino group. CAR can form both tetrahedral and octahedral types of complexes, but their exact configuration depends on the size of the metal cation, ligand-to-metal ratios, and ionic strength of the supporting electrolyte.[1] In this regard, the thermodynamic behavior of Ca^{2+}, Mg^{2+}, Cu^{2+}, Mn^{2+}, Zn^{2+}, and Pb^{2+}-CAR systems was recently elucidated.[2,5,11] Therefore, the present study focused on the determination of the thermodynamic interaction parameters of CAR with Hg^{2+} and Cd^{2+} by means of potentiometry in NaCl aqueous solutions with different ionic strengths ($0.15 \leq I$/mol $L^{-1} \leq 0.96$) and temperatures ($288.15 \leq T/K \leq 310.15$).

Considering the advantageous complexing ability of CAR and its poorly detailed electrochemical properties,[1,12–14] we synthesized the ferrocenyl-carnosine (FcCAR, Fig. 1) as an electroactive CAR derivative for metal cation sensing applications. The conjugation of aminoacids and proteins with ferrocene units is well exploited in the literature leading to redox-active materials with interesting electron-transfer properties.[15–17] The functionalization of the amine group of the β-alanine residue did not affect the multiple recognition sites of CAR (*i.e.*, imid-

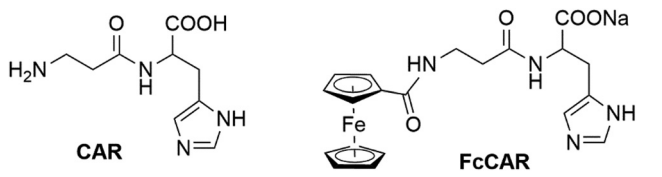

Fig. 1 Chemical structures of L-carnosine (CAR) and the newly synthesized ferrocenyl-carnosine (FcCAR).

[a]*Dipartimento di Scienze Chimiche, Biologiche, Farmaceutiche ed Ambientali, Università di Messina, Viale Ferdinando Stagno d'Alcontres 31, 98166 Messina, Italy. E-mail: cfoti@unime.it*
[b]*Nanobiotechnology & Bioanalysis Group, Departament d'Enginyeria Química, Universitat Rovira i Virgili, Avinguda Països Catalans 26, 43007 Tarragona, Spain*
[c]*Consiglio Nazionale delle Ricerche, Istituto per lo Studio dei Materiali Nanostrutturati (CNR-ISMN), URT di Messina c/o Dipartimento di Scienze Chimiche, Biologiche, Farmaceutiche ed Ambientali, Università di Messina, Viale Ferdinando Stagno d'Alcontres 31, 98166 Messina, Italy*

† Electronic supplementary information (ESI) available. See DOI: https://doi.org/10.1039/d2dt04093j

azole ring and amino and carboxylic groups) and meanwhile strengthened the electrochemical applications of CAR by the redox-active ferrocene unit.[18–21] FcCAR was synthesized by a coupling reaction between *N*-hydroxysuccinimide activated ferrocene and CAR in the presence of sodium bicarbonate and it was characterized by analytical and spectroscopic techniques. To the best of our knowledge, no reports of ferrocene–carnosine conjugates, which may offer the potential for the development of metal specific probes, have been described in the literature. In this paper, we provide a full account of the complexing ability of CAR together with the spectroscopic and electrochemical properties of the first ferrocene–carnosine conjugate (FcCAR) with the aim to evaluate its sensing properties.

Experimental

Materials

L-Carnosine (CAR) solutions were prepared by weighing the corresponding Sigma Aldrich product without further purification, and their purity was checked by potentiometry (≥99.0%). Pb^{2+} solutions were prepared by weighing the corresponding salts, lead nitrate, $Pb(NO_3)_2$ (Fluka, ≥99.0%), for UV-vis spectrophotometric measurements, and lead acetate trihydrate, $Pb(CH_3OO)_2{\cdot}3H_2O$ (Sigma Aldrich, ≥99.0% A.C.S. Reagents), for voltammetric measurements. Cd^{2+} and Hg^{2+} solutions were prepared by weighing cadmium chloride, $CdCl_2$ (Fluka, ≥99.0%), and mercury chloride, $HgCl_2$ (Riedel-de Haën, 99.5%), products. The Pb^{2+}, Cd^{2+} and Hg^{2+} solutions were standardized by titrations with EDTA (ethylenediaminetetraacetic acid disodium salt, Sigma Aldrich, BioUltra, ≥99.0%) standard solution. Sodium hydroxide, NaOH, and hydrochloric acid, HCl, solutions were prepared from Fluka concentrated vials and titrated respectively with potassium biphthalate and sodium carbonate, and dried in an oven at 383.15 K for at least an hour before their use. The sodium hydroxide solutions were always stored in dark bottles to preserve them with air CO_2 using soda lime traps. The sodium chloride, NaCl, solutions were prepared by weighing the corresponding salt (Sigma Aldrich®, puriss.), previously dried in an oven at 383.15 K. Potassium chloride, KCl (Scharlau, extra pure), and sulfuric acid, H_2SO_4, (EPR, >95.0–98.0%), were also used. Potassium ferricyanide, $K_3Fe(CN)_6$ (powder, <10 micron, 99+%), ferrocenecarboxylic acid (>96.0%), *N*,*N*-dimethylformamide (DMF) anhydrous (99.8%), and diethyl ether anhydrous (≥99.7%) were purchased from Sigma Aldrich (Spain) and used as received. Tetrahydrofuran, THF (Acroseal, Acros Organics, 99.8%, extra dry), *N*,*N*′-dicyclohexylcarbodiimide (DCC), *N*-hydroxysuccinimide (NHS) (Fluka Analytical, puriss. ≥99.0%), sodium hydrogen carbonate, $NaHCO_3$ (Panreac), and acetone, ACS BASIC (Scharlau), were used as received. MOPS buffer was prepared by weighing 3-(*N*-morpholino)propanesulfonic acid, 4-morpholinepropanesulfonic acid (MOPS, Sigma Aldrich, minimum ≥99.5% (titration)) and the corresponding Scharlau salts, sodium acetate anhydrous (CH_3COONa, extra pure) and EDTA dehydrate. Solutions were prepared with bidistilled water (conductivity <0.1 μS cm^{-1}) obtained from a Milli-Q® system (Millipore, Madrid, Spain).

Potentiometric equipment and procedure

Potentiometric measurements were performed using a Metrohm model 809 Titrando potentiometric system, equipped with an LL-Unitrode WOC combined glass electrode and a Metrohm Dosino 800 automatic dispenser. This PC-automated titration system provided experimental data. The titrant delivery employed a Metrohm TiAMO 2.2 software to estimate the error of the potentiometric system, which was ±0.15 mV for e.m.f. and ±0.002 mL for titrant volume readings, respectively.

Potentiometric titrations were performed by adding NaOH standard to 25 mL of CAR solutions ($1 \leq C_L/\text{mmol L}^{-1} \leq 6$), containing Hg^{2+} or Cd^{2+} ($0.5 \leq C_M/\text{mmol L}^{-1} \leq 3$), HCl ($5 \leq C_H/\text{mmol L}^{-1} \leq 12$) and NaCl ($0.15 \leq C_{NaCl}/\text{mol L}^{-1} \leq 0.96$). Measurements were carried out at constant temperature ($288.15 \leq T/\text{K} \leq 310.15$) using thermostated glass jacket cells, under constant magnetic stirring and nitrogen bubbling in order to ensure homogeneity of the systems and avoid possible interferences of air O_2 and CO_2 inside. To determine the standard electrode potential, $E°$, and pK_w values, independent titrations of HCl with standard NaOH solutions were carried out for each measurement under the same experimental conditions of ionic strength and temperature. The potentiometric data were elaborated using BSTAC4 and STACO4 computer programs.[22] Both determined the purity of the reagents, formal potential, $E°$, the liquid junction potential coefficient j_a, $E_j = j_a[H^+]$ and formation constants of the species. Speciation diagrams were obtained by means of the HySS program.[23]

UV-vis spectrophotometric equipment and procedure

Spectrophotometric measurements were performed using a Varian Cary 50 UV-vis spectrophotometer equipped with an optic fiber probe, having a fixed 1 cm path length. The experimental data (absorbance *vs*. wavelength) were acquired using a Varian Cary WinUV (model 3.00) software, which controls some of the main parameters, such as the wavelength range, scanning speed and baseline correction. Simultaneously, a Metrohm 713 potentiometer connected to a combined glass electrode (Ross type 8102, from Thermo/Orion) was used to measure the pH of the solutions. Both A *vs*. λ (nm) and pH *vs*. volume of titrant (mL) data were acquired. The titrant delivered in the cell was measured by means of a Metrohm 665 Dosimat, and the temperature was kept constant at T = 298.15 ± 0.10 K by using thermostated glass jacket cells. Solutions were vigorously stirred to ensure the homogeneity of the system, while pure nitrogen (N_2) was bubbled in the solutions to exclude the possible presence of O_2 and CO_2 inside.

As the potentiometric measurements, the spectrophotometric measurements were carried out as titrations in a wide selected wavelength range ($200 \leq \lambda \leq 400$ nm). For acid–base studies, 25 mL of solutions containing FcCAR ($0.04 \leq C_L/\text{mmol L}^{-1} \leq 0.15$), HCl (3 mmol L^{-1}), and NaCl (I = 0.15 mol

L^{-1}) were titrated with standard NaOH in the pH range 3–9.5. For metal complex studies, 25 mL of the solutions containing FcCAR ($0.02 \leq C_L$/mmol $L^{-1} \leq 0.04$), Hg^{2+} or Pb^{2+} ($0.01 \leq C_M$/mmol $L^{-1} \leq 0.02$, varying the metal : ligand ratio $0.5 \leq C_M/C_L \leq 2$), HCl (0.2 mmol L^{-1}) and NaCl (I = 0.15 mol L^{-1}) were titrated with standard NaOH in the $3 \leq$ pH ≤ 9.5 pH range.

The spectrophotometric data were elaborated using the HYSPEC computer program[24] able to analyze the UV-vis spectra, determining the formation constants of the species, as well as the molar absorption coefficients.

Voltammetric equipment and procedure

Electrochemical measurements were carried out in KCl (0.1 mol L^{-1}) aqueous solutions and at room temperature, using two PC-controlled electrochemical workstations: (i) PNT-10-Autolab potentiostat–galvanostat and (ii) μAutolab potentiostat–galvanostat type III (Eco Chieme) with an IME663 interface, both equipped with Metrohm DropSens Screen-Printed Electrodes (SPEs) (Model DRP-110). Voltammograms were deconvoluted using a General Purpose Electrochemical System (GPES), version 4.9 by Eco Chemie B.V. processing software.

The redox properties of FcCAR were assessed by Cyclic Voltammetry (CV) and Differential Pulse Voltammetry (DPV) in the potential range −1 to +1 V (*vs.* Ag/AgCl) in 0.1 mol L^{-1} KCl. Metal solutions were prepared in MOPS buffer (pH = 7). CV was performed at 0.1 V s^{-1}. DPV parameters were set as follows: increment potential of each pulse = 0.01 V, amplitude = 0.1 V, pulse width = 0.05, sample width = 0.0025 s and pulse period = 0.1 s.

Synthesis of ferrocenyl-carnosine (FcCAR)

A solution of ferrocenecarboxylic acid (**1**) (655 mg; 2.85 mmol) and NHS (360 mg; 3.13 mmol) in 30 mL of anhydrous THF was added to a stirring solution of DCC (603.8 mg; 2.93 mmol) in 10 mL of THF. The mixture was stirred at room temperature for 24 h; the brown solid was removed by filtration and the organic solvent was evaporated to give the ferrocenic ester of *N*-hydroxysuccinimide (**2**). The chemical structure and the purity of (**2**) were confirmed by ^{1}H-NMR analyses and compared to literature data.[25]

The ferrocenyl intermediate (**2**) (821 mg; 2.50 mmol) was dissolved in DMF (25 mL) and slowly added, under stirring, in an ice bath, to a CAR (678.9 mg; 3.0 mmol), $NaHCO_3$ (210.3 mg; 2.50 mmol) and H_2O/DMF (1 : 1) solution. The reaction mixture was stirred at room temperature for 20 h. The solvent was evaporated under vacuum and the brown solid was purified by crystallization from water/acetone to obtain FcCAR (**3**) in 64% overall yield.

NMR and mass analyses

^{1}H and ^{13}C NMR spectra of FcCAR were recorded in D_2O on an Agilent 500 MHz spectrometer at room temperature (r.t.). The ^{13}C NMR spectrum was recorded adding acetone as an internal standard fixing the methyl carbon signal at δ 31. The mass spectra were obtained in positive-ion mode, and in direct infusion, using an ESI-mass spectrometer API-2000 (AB Sciex).

^{1}H NMR (D_2O, 500 MHz): δ 7.66 (s, 1H), 6.85 (s, 1H), 4.27 (m, 2H), 4.20 (m, 2H), 4.04 (m, 1H), 3.96 (m, 5H), 3.13–2.93 (m, 2H), 2.90–2.78 (m, 2H), 2.37–2.26 (m, 2H). ^{13}C NMR (D_2O : acetone-d_6, 125 MHz): δ 179.22, 174.73, 173.01, 136.90, 134.28, 118.86, 71.53, 56.57, 56.34, 37.30, 37.23, 33.56. ESI-MS (m/z): 439.10 detected as $[MH]^+$ species cld for $C_{20}H_{22}FeN_4O_4$ (m/z: 438.099).

Results and discussion

Thermodynamic interaction parameters for Hg^{2+}- and Cd^{2+}-CAR systems

As mentioned earlier, CAR is able to coordinate to a number of bivalent metal cations.[1,2,11] To evaluate the interactions with Hg^{2+} and Cd^{2+}, speciation studies were experimentally performed by potentiometric titrations under different conditions of ionic strength, temperature and metal–ligand concentration ratio. In the calculation of the complex formation constants, literature values of protonation constants of CAR, hydrolysis constants of the metal cations and formation of chloride species were taken into account.[2,26–28]

The most reliable speciation models for both systems were chosen on the basis of general criteria, such as simplicity, standard and mean deviation of the fit, as well as formation percentage of species.[29,30] The experimental formation constant values of the Hg^{2+}- and Cd^{2+}-CAR species, under different conditions of temperature and ionic strength, are listed in Table 1 and expressed as global formation constants, β, which refers to the following reaction:

$$M^{2+} + iH^+ + L^- = MH_iL^{2+i-1} \quad (1)$$

Formation of three complex species, namely HgL^+, $HgLH^{2+}$, and $HgLOH^0$ for the Hg^{2+}-CAR system and CdL^+, $CdLH^{2+}$ and $CdLH_2^{3+}$ for Cd^{2+}-CAR was found. The stability of ML and MLH species increases as the ionic strength grows and, *vice versa*, it decreases from T = 288.15 K to T = 310.15 K. The $HgLOH^0$ species shows a different behavior, as well as $CdLH_2^{3+}$, whose quantity was only relevant at I = 0.15 mol L^{-1} and T = 298.15 K, and negligible under the other conditions.

The speciation profile relating to the Hg^{2+}-CAR system (Fig. 2a) better highlights the formation of the metal complex species throughout the pH, proving the binding ability of CAR towards the metal cations at I = 0.15 mol L^{-1} and T = 298.15 K. The high stability constants of Hg^{2+}-CAR allowed the suppression of the hydrolysis of the metal cation. Instead, the Hg^{2+}-Cl^- species prevailed up to pH ≅ 5. The HgL^+ species formed starting from pH ≅ 5.5, reaching a 0.47 mole fraction at pH ≅ 7.5 in NaCl aqueous solution (C_M = 2 mmol L^{-1} and C_L = 4 mmol L^{-1}). A minor fraction of the $HgLH^{2+}$ complex was found at $4 \leq$ pH ≤ 9. The $HgLOH^0$ species was present starting from pH ≅ 6.5 and totally prevailed at pH = 9. The distribution concerning the Cd^{2+}-CAR system (Fig. 2b) was noticeably different, due to the lower formation percentage of the species,

Table 1 Experimental formation constant values of Hg^{2+}- and Cd^{2+}-carnosine (L) species in NaCl aqueous solutions

		$\log \beta^a$					
M	Species	$I = 0.15^b$ $T = 298.15$ K	$I = 0.49^b$	$I = 0.72^b$	$I = 0.96^b$	$I = 0.15^b$ $T = 288.15$ K	$I = 0.15^b$ $T = 310.15$ K
Hg^{2+}	ML^+	17.28 ± 0.01[c]	17.61 ± 0.02[c]	18.08 ± 0.03[c]	18.36 ± 0.01[c]	17.49 ± 0.08[c]	16.81 ± 0.02[c]
	MLH^{2+}	24.37 ± 0.02	25.20 ± 0.04	26.03 ± 0.07	25.60 ± 0.07	25.26 ± 0.02	23.63 ± 0.07
	$MLOH^0$	9.46 ± 0.03	8.90 ± 0.02	9.03 ± 0.02	9.07 ± 0.02	10.38 ± 0.04	8.95 ± 0.02
Cd^{2+}	ML^+	3.11 ± 0.07	3.68 ± 0.05	3.90 ± 0.05	4.13 ± 0.06	4.22 ± 0.04	3.42 ± 0.08
	MLH^{2+}	12.17 ± 0.03	12.69 ± 0.03	12.96 ± 0.06	13.15 ± 0.03	13.07 ± 0.03	11.80 ± 0.08
	MLH_2^{3+}	18.85 ± 0.03	—	—	—	—	—

[a] Refers to reaction (1). [b] Expressed in mol L^{-1}. [c] ≥95% of confidence interval.

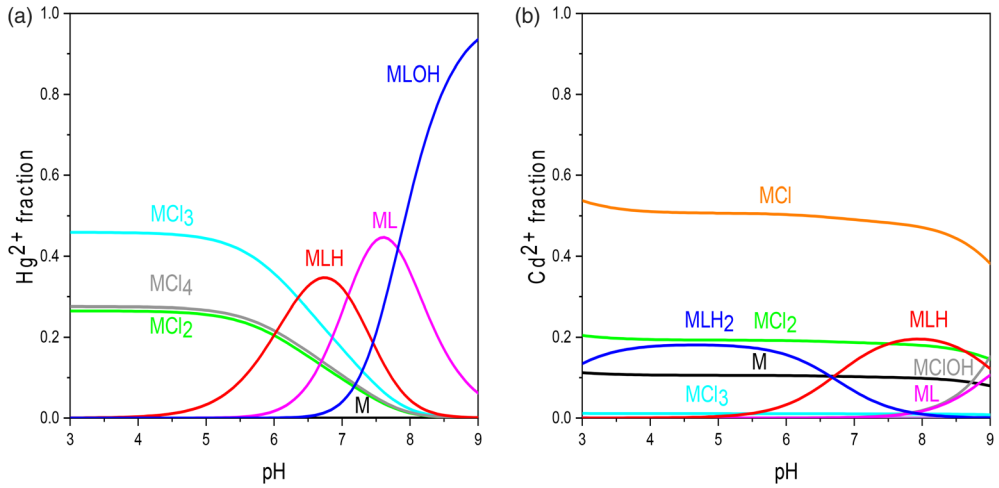

Fig. 2 Speciation diagrams *vs.* pH of (a) Hg^{2+}- and (b) Cd^{2+}-CAR (L) species (charges omitted for simplicity) in NaCl aqueous solution at I = 0.15 mol L^{-1} and T = 298.15 K (C_M = 2 mmol L^{-1}; C_L = 4 mmol L^{-1}).

which was always below 0.2. An amount of free cadmium (0.1 metal fraction) was always present, as well as the Cd^{2+}-Cl^- species.

The formation constants of Table 1 were used to study the dependence on ionic strength and temperature following the Debye–Hückel type (2) and van't Hoff (3) equations, respectively:[31–33]

$$\log \beta = \log \beta^0 - 0.51 \cdot z^* \frac{\sqrt{I}}{1 + 1.5\sqrt{I}} + CI \quad (2)$$

$$\log \beta^T = \log \beta^\theta + \Delta H(1/\theta - 1/T)R \ln 10 \quad (3)$$

In eqn (2), β and β^0 correspond to the stability constants at a given ionic strength and infinite dilution respectively, $z^* = \sum(\text{charge})^2_{\text{reactants}} - \sum(\text{charge})^2_{\text{products}}$, and C is an empirical parameter. In eqn (3), $\log \beta^T$ is the stability constant at a given temperature T (expressed in Kelvin) and ionic strength, $\log \beta^\theta$ is the value at the reference temperature θ (T = 298.15 K) and R = 8.314472 J K^{-1} mol^{-1} when ΔH is expressed in kJ mol^{-1}. The calculated values of $\log \beta^0$ and C, for the dependence on ionic strength, and ΔH, for the dependence on temperature, are reported in Table 2. In the same table, calculated ΔG ($\Delta G = -RT \ln \beta$) and $T\Delta S$ ($T\Delta S = \Delta H - \Delta G$) values are also reported to have a complete thermodynamic picture. All the enthalpy change values (ΔH) concerning the formation of Hg^{2+} and Cd^{2+}-CAR species involved exothermic processes, along with negative entropy change values ($T\Delta S$). Among them, the ML species for the Hg^{2+}-CAR system was the only one with a positive $T\Delta S$, suggesting a rise of the order due to the solvation processes. The thermodynamic parameters reported in Table 2 are very useful for predictive purposes allowing the calculation of the formation constants at any value of ionic strength and temperature in the range $0 \le I$/mol $L^{-1} \le 1$ and $278.15 \le T$/K ≤ 318.15. In Table 2, thermodynamic parameters concerning the formation of the Pb^{2+}-CAR system, previously determined, are also reported,[11] useful for later considerations.

On the basis of the thermodynamic interaction parameters, the sequestering ability of CAR towards the two metal cations can be quantitatively assessed by the calculation of $pL_{0.5}$. The latter is an empirical parameter that allows the quantification of the ability of a ligand to sequester a metal cation under specific conditions of temperature, ionic strength and pH. The $pL_{0.5}$ corresponds to the cologarithm of the needed ligand concentration to bind 50% of the metal cation in traces, and it is

Table 2 Thermodynamic formation parameters (eqn (2) and (3)) for the Hg^{2+}- and Cd^{2+}-CAR (L) species in NaCl at T = 298.15 K

M	Species	$\log \beta^{0\,a}$	C	$\Delta G^{a,b,c}$	$\Delta H^{a,b,c}$	$T\Delta S^{a,b,c}$
Hg^{2+}	ML	17.54 ± 0.01[d]	1.8 ± 0.1[d]	−98.6	−65 ± 10[d]	34
	MLH	24.42 ± 0.02	2.1 ± 0.2	−139.1	−162 ± 14	−23
	MLOH	9.75 ± 0.01	0.1 ± 0.1	−54.0	−118 ± 11	−64
Cd^{2+}	ML	3.44 ± 0.12	1.6 ± 0.2	−17.8	−60 ± 40	−42
	MLH	12.26 ± 0.11	1.4 ± 0.2	−69.5	−98 ± 30	−29
$Pb^{2+\,e}$	ML_2	9.93	−0.24	−56.7	−122	−65
	ML_2H	18.91	−0.24	−107.9	−87	21

[a] Refers to reaction (1). [b] In kJ mol^{-1}. [c] At I = 0.15 mol L^{-1} (NaCl). [d] ≥95% of confidence interval. [e] Ref. 11.

determined by the following sigmoidal Boltzmann type equation with asymptotes equal to 1 for pL → −∞ and 0 for pL → +∞:[31,34]

$$\chi = \frac{1}{1 + 10^{(pL - pL_{0.5})}} \quad (4)$$

where χ represents the sum of mole fractions of the metal–ligand species and pL is the cologarithm of the total ligand concentration. The greater the $pL_{0.5}$ values, the greater the sequestering ability.

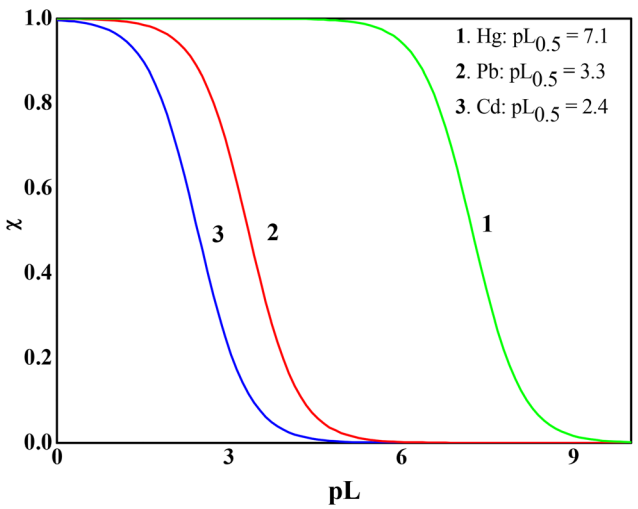

Fig. 3 Sequestration diagram of CAR towards Hg^{2+}, Pb^{2+} and Cd^{2+} ions at pH = 8.1, I = 0.7 mol L^{-1} and T = 273.15 K.

An example of the sequestering diagram under conditions simulating seawater (*i.e.*, I = 0.7 mol L^{-1} and pH = 8.1, at T = 273.15 K) is reported in Fig. 3. In the diagram, along with Hg^{2+} and Cd^{2+}, Pb^{2+} is also reported, whose interactions with CAR were recently studied[11] and are provided in Table 2. As can be observed, the highest sequestering ability of CAR is towards Hg^{2+}, following the trend:

$$Hg^{2+} \gg Pb^{2+} > Cd^{2+}$$

With this in mind, we synthesized an electroactive CAR derivative (FcCAR) with the aim to evaluate its use as a sensor for Pb^{2+} and Hg^{2+}. We did not consider Cd^{2+} cation since it is less involved in the coordination with CAR molecule.

Synthesis and characterization of ferrocenyl-carnosine (FcCAR)

The redox-active ferrocene carnosine derivative (FcCAR, **3**) was synthesized by a coupling reaction of free CAR with the *N*-hydroxysuccinimide-activated ferrocene (**2**) under mild experimental conditions (Scheme 1). The ferrocenecarboxylic acid (**1**) was activated with NHS to form **2** which was treated at room temperature with CAR in the presence of sodium bicarbonate to afford FcCAR (**3**) in 64% overall yield. Given the amphiphilic characteristics of FcCAR, the selection of a suitable mixture of water/aprotic solvents for the coupling reaction (*i.e.*, water/DMF) and for the subsequent purification (crystallization from water/acetone) was crucial for the success of the synthesis. The ^{1}H NMR spectrum confirmed the structure of FcCAR showing three distinct regions of signals: the imidazole protons of the histidine residue (7.66–6.85 ppm); the typical

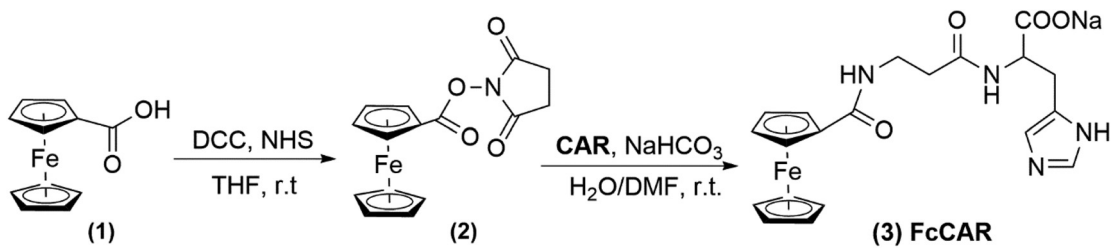

Scheme 1 Synthetic scheme for the preparation of ferrocenyl-carnosine (FcCAR).

Table 3 Protonation constant values of CAR and FcCAR in NaCl aqueous solution at I = 0.15 mol L^{-1} and T = 298.15 K

Reaction	CAR[a] log β	FcCAR
$H^+ + L^- = HL^0$	9.38	6.45 ± 0.04[b]
$2H^+ + L^- = H_2L^+$	16.17	9.45 ± 0.06
$3H^+ + L^- = H_3L^{2+}$	18.86	—
	log K	
$H^+ + L^- = HL^0$	9.38	6.45
$H^+ + HL^0 = H_2L^+$	6.79	3.00
$H^+ + HL^+ = H_3L^{2+}$	2.69	—

[a] Ref. 2. [b] ≥95% of confidence interval.

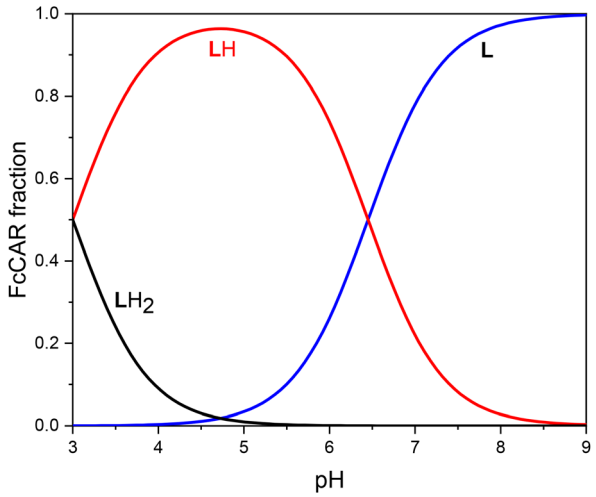

Fig. 4 Speciation diagram *vs.* pH of FcCAR (L) species (charges omitted for simplicity) in NaCl aqueous solution at I = 0.15 mol L^{-1} and T = 298.15 K (C_L = 0.1 mmol L^{-1}).

peaks of ferrocene (4.27–3.96 ppm) and the peaks between 3.13 and 2.26 ppm of the peptidyl moiety.

Acid–base properties and complexing ability of FcCAR

FcCAR has two ionizable groups, consisting of the carboxylic group and the imidazole ring. The study of equilibria in solution was performed by UV-vis spectrophotometric titrations from pH ≈ 3 to 9 (Fig. S1, ESI†). The UV-vis spectrum of FcCAR is characterized by a broad band at around 205 nm and a small one at around 260 nm, which are attributable to n–π* and π–π* electronic transitions, respectively. As the pH increases, and thus the deprotonation degree of the molecule, a gradual gain in absorbance occurs. Moreover, the ε of the deprotonated FcCAR species is also higher with respect to those of the protonated ones (Fig. S2, ESI†). The protonation constant values obtained by using the HYSPEC program are listed in Table 3 along with those of CAR, previously determined.[2] In the same table, stepwise formation constants are also presented because they are useful in evaluating the functional groups involved in each protonation equilibrium. CAR has three protonation constants corresponding to the protonation of the amino group of the β-Ala residue (log K = 9.38), the nitrogen of the imidazole ring (log K = 6.79) and the carboxylate (log K = 2.69). In FcCAR molecule, the amino group of the β-Ala residue is conjugated with the Fc moiety and the first protonation step involves the imidazole ring (log K = 6.45), while the second one the carboxylic group (log K = 3.00). The distribution diagram of FcCAR (Fig. 4) shows that for 5 ≤ pH ≤ 8, the range of interest for most natural fluids, FcCAR is present as HL^0 and L^- species, whose formation reaches a maximum at pH = 5 and 9, respectively.

Once the FcCAR acid–base behavior was defined, UV-Vis titrations were performed in the presence of metal cations in order to evaluate the strength of the interactions with Hg^{2+} and Pb^{2+}. In particular, in the presence of Hg^{2+}, the UV-vis

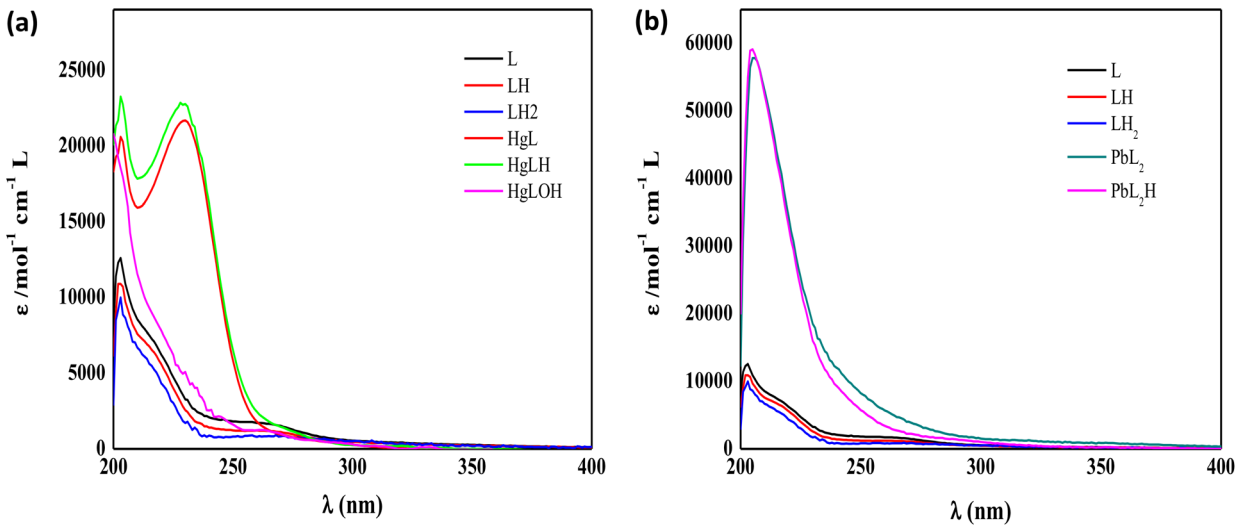

Fig. 5 ε *vs.* λ of the (a) Hg^{2+}- and (b) Pb^{2+}-FcCAR (L) species (charges omitted for simplicity) in NaCl aqueous solution at I = 0.15 mol L^{-1} and T = 298.15 K.

Table 4 Experimental formation constant values of Hg^{2+}- and Pb^{2+}-FcCAR (**L**) species, in comparison with Hg^{2+}- and Pb^{2+}-CAR species, at I = 0.15 mol L^{-1} (NaCl) and T = 298.15 K

M	Species	$\log \beta^a$	
		CAR	FcCAR
Hg^{2+}	ML	17.54 ± 0.01[b]	18.72 ± 0.02[b]
	MLH	24.42 ± 0.02	24.85 ± 0.04
	MLOH	9.75 ± 0.01	9.81 ± 0.06
Pb^{2+}	ML_2	9.93[c]	16.29 ± 0.08
	ML_2H	18.91[c]	23.19 ± 0.04

[a] Refers to reaction (1). [b] ≥95% of confidence interval. [c] Ref. 11.

spectra of the molecule were affected by a significant variation as reported in Fig. 5, where ε *vs.* λ values of the Hg^{2+} and Pb^{2+}-**L** species are shown. This could be probably due to the involvement of the imidazole ring in the complexation. Indeed, the most trustworthy speciation model for the Hg^{2+}-FcCAR system is reported in Table 4 and provides the formation of three complex species, namely ML, MLH and MLOH. The behavior of the Pb^{2+}-FcCAR system is different, and the formation of two ML_2 and ML_2H complex species (Table 4) was achieved without, therefore, the involvement of the imidazole ring. In this case, we observed only the increase in absorbance, but the spectrum shape remained unchanged. For both systems, the speciation diagrams in Fig. 6 describe a strong chelating ability of FcCAR towards two metal cations. In particular, the Hg^{2+} fraction reached a maximum of 0.9 in the formation of the MLH and ML species at

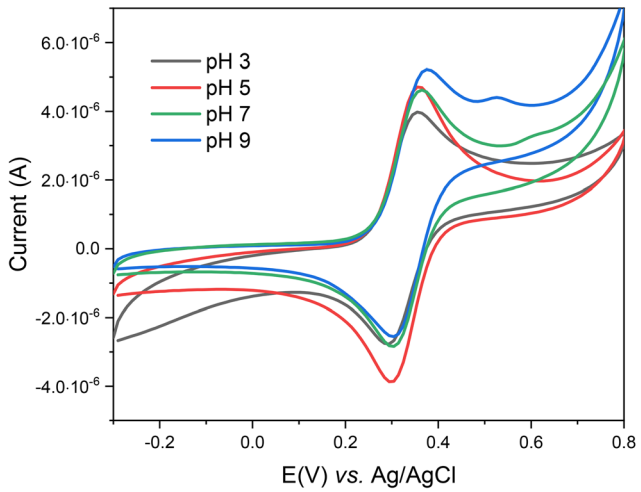

Fig. 7 CVs of FcCAR (1 mmol L^{-1}) in 0.1 mol L^{-1} KCl aqueous solution at different pH values (3 ≤ pH ≤ 9) and room temperature (scan rate = 0.1 V s^{-1}).

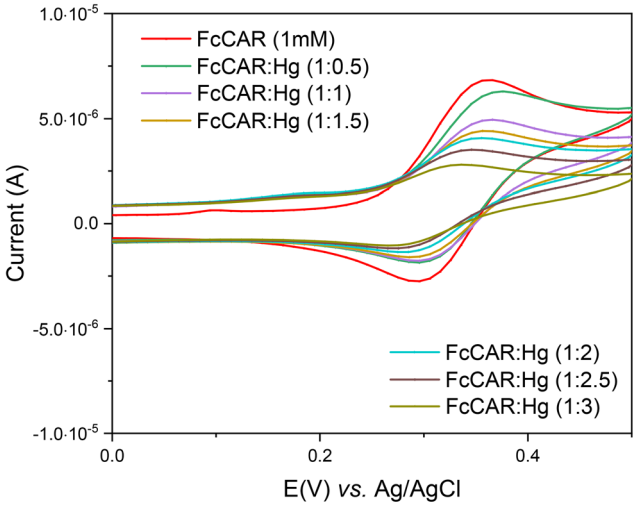

Fig. 8 CV titrations of FcCAR (1 mmol L^{-1}) with Hg^{2+} in 0.1 mol L^{-1} KCl aqueous solution at pH = 7 and room temperature (scan rate = 0.1 V s^{-1}).

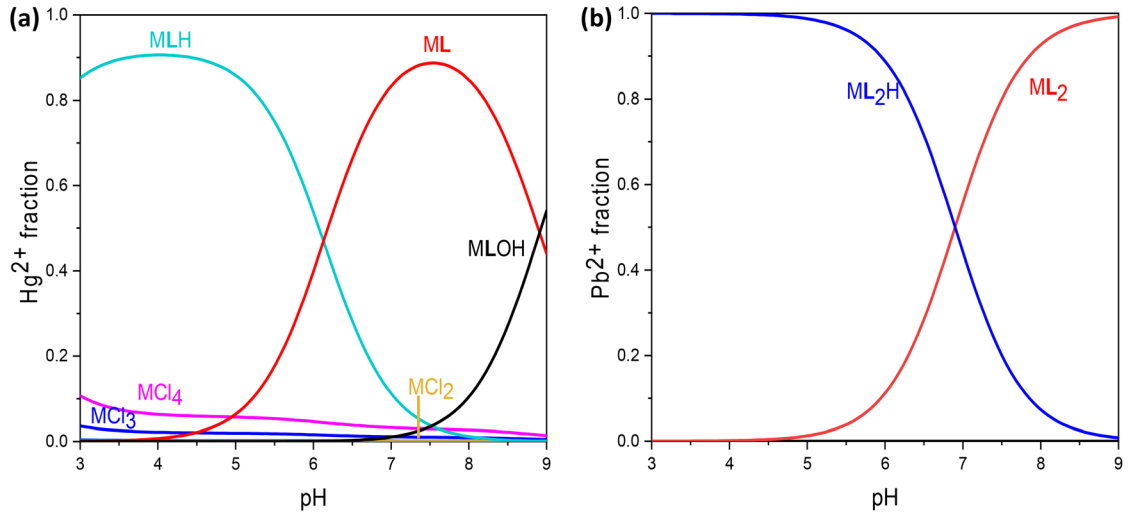

Fig. 6 Speciation diagrams *vs.* pH of (a) Hg^{2+}- and (b) Pb^{2+}-FcCAR (**L**) species (charges omitted for simplicity) in NaCl aqueous solution at I = 0.15 mol L^{-1} and T = 298.15 K (C_M = 2 mmol L^{-1}; C_L = 4 mmol L^{-1}).

$3 \leq pH \leq 5$ and $7 \leq pH \leq 8$, respectively. The MLOH species formed starting from pH ≥ 7. On the other hand, Pb^{2+} was totally coordinated by FcCAR as PbL_2H or PbL_2.

The high complexing capacities of FcCAR were also reflected in the sequestering abilities, calculated using eqn (4). The comparison of the sequestering ability of CAR and FcCAR with respect to Pb^{2+} and Hg^{2+} is shown in Fig. S3 of the ESI.† For both systems, an increase in the $pL_{0.5}$ value of at least three orders of magnitude was obtained.

Electrochemistry of FcCAR

To evaluate the sensing properties of FcCAR with regard to Hg^{2+} and Pb^{2+}, voltammetric measurements were performed. The electrochemical responses of Screen-Printed Electrodes (SPEs) were assessed by means of Cyclic Voltammetry (CV) using 1 mmol L^{-1} $[Fe(CN)_6]^{3-}$ in KCl (I = 0.1 mol L^{-1}) aqueous solution and room temperature. Scan rate: 0.1 V s^{-1}.

The redox properties of FcCAR were investigated by means of CV at different potential windows ($-1.0 \leq E(v)$ *vs.* Ag/AgCl $\leq +1.0$), pH ($3 \leq pH \leq 9$ at scan rate: 0.1 V s^{-1}) and scan rate ranges ($10 \leq$ mV $s^{-1} \leq 100$ at pH = 7 (Fig. 7 and Fig. S4†). As can be observed in Fig. 7, there are small ΔE_p variations as the pH changes in the CVs as a function of pH. While the cathodic peaks remain essentially unchanged, anodic peaks are anodically displaced by 20 mV from pH 3 to pH 9, indicating a slight hindrance in the oxidation of Fc due to deprotonation of the carnosine residue. Interestingly, the CV of FcCAR revealed the appearance of a small oxidation peak at ~0.6 V and pH 7 that is displaced to lower potentials as the pH increases (0.526 V at pH = 9). This peak is due to the oxidation of the imidazole

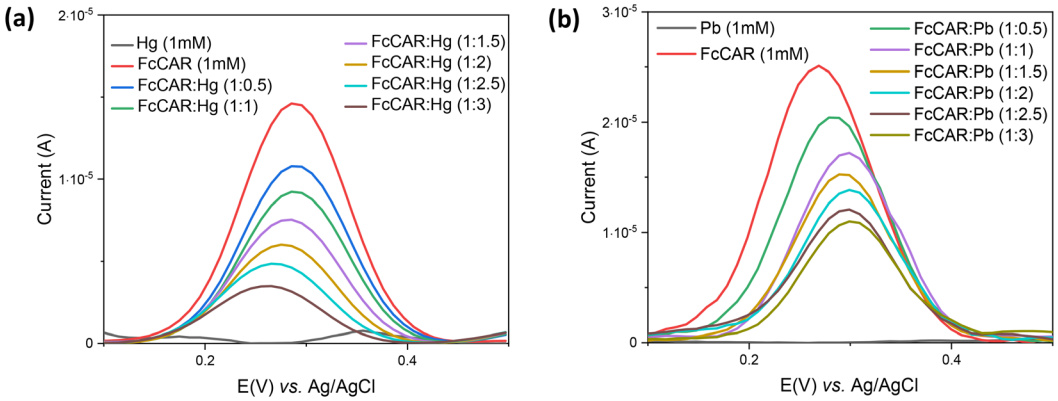

Fig. 9 DPV titrations of FcCAR (1 mmol L^{-1}) with (a) Hg^{2+} and (b) Pb^{2+} in 0.1 mol L^{-1} KCl aqueous solution at pH = 7 and room temperature.

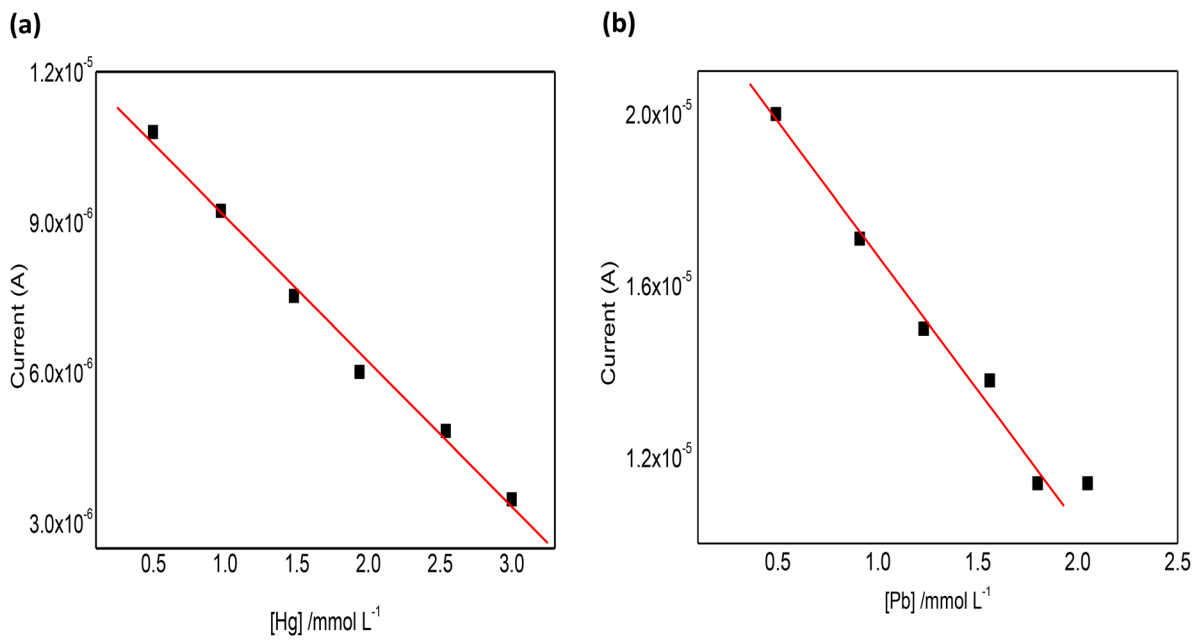

Fig. 10 Dependence of the cathodic peak current of FcCAR in 0.1 mol L^{-1} KCl aqueous solution *vs.* (a) Hg^{2+} and (b) Pb^{2+} concentrations (pH = 7, room temperature, C_L = 1 mmol L^{-1}, $0.5 \leq C_M$ mmol $L^{-1} \leq 3$).

ring of carnosine, as reported in the literature,[13] which is favored as deprotonation of the imidazole ring occurs.

To evaluate the FcCAR sensing activity, electrochemical titrations were performed by adding Hg^{2+} or Pb^{2+} ($0.5 \leq C_M$/mmol $L^{-1} \leq 3$, in MOPS buffer at pH = 7) to FcCAR solutions. CV and DPV titrations were performed in a narrower potential range ($-0.5 \leq E$(v) *vs.* Ag/AgCl $\leq +0.5$), further restricted in Fig. 8 and 9 to focus only on the FcCAR signal. As can be observed, FcCAR peaks decrease in intensity as the metal concentration increases. The trend of cathodic peak currents *vs.* metal concentration is underlined in Fig. 10. The peak current linearly decreases in the ranges $0.5 \leq C_M$/mmol $L^{-1} \leq 3.0$ for Hg^{2+} and $0.5 \leq C_M$/mmol $L^{-1} \leq 1.7$ for Pb^{2+}. This decrease may be due to the coordination of both heavy metals to the CAR moiety, which markedly increases the molecular weight of the complex and reduces its diffusion coefficient and, hence, the peak current. In the case of addition of Hg^{2+}, the peak potentials are not changed up to a 1 : 1 stoichiometry and are then cathodically shifted. This suggests that the coordination of this cation to FcCAR promotes its oxidation by stabilizing the electrogenerated ferrocenium cation in the anionic Hg-FcCAR complex or by being reduced to Hg^{+}.[35] In contrast, the Pb^{2+} complex is neutral and oxidation of Fc destabilizes the complex by electrostatic repulsion with the metal center, provoking an anodic shift of the peak potential even for substoichiometric M:L molar ratios.[36] This voltametric behavior suggests that FcCAR could be used as a signal-off detection system for heavy metals.

Conclusions

The widely studied interactions of CAR with bivalent metal cations allowed us to elucidate its advantageous complexing ability, unlike its electrochemical properties. In this regard, taking into account that CAR has multiple recognition groups and, on the other hand, the ferrocene moiety can be easily functionalized,[19] a more electroactive and versatile product was synthesized, namely FcCAR, and tested as a potential metal cation probe with the aim of deepening the study towards potentially toxic metal cations. First of all, a comprehensive thermodynamic investigation on the interactions of CAR with Hg^{2+} and Cd^{2+} was performed. This preliminary potentiometric study was crucial to assess a steady speciation model and to evaluate the sequestering ability of CAR towards the metal cations. In light of this, the potential use of CAR as a sensor was evaluated with respect to Hg^{2+} and Pb^{2+} (whose speciation study had recently been reported[11]), while Cd^{2+} was not considered due to the low complexing ability of CAR towards this metal cation. A synergic UV-vis spectrophotometric and voltammetric study was carried out both on Hg^{2+}- and Pb^{2+}-FcCAR systems. Spectrophotometric measurements elucidated the strength of metal–ligand interactions. Voltammetric measurements, performed by means of CV and DPV on Screen-Printed Electrodes, inspected its sensing ability. Electrochemical results have been shown to be promising for the electrochemical detection of these metal cations in aqueous environment.

Conflicts of interest

There are no conflicts to declare.

References

1 M. L. Branham, P. Singh, K. Bisetty, M. Sabela and T. Govender, *Molecules*, 2011, **16**, 10269–10291.
2 C. Abate, G. Cassone, M. Cordaro, O. Giuffrè, V. Mollica-Nardo, R. C. Ponterio, F. Saija, J. Sponer, S. Trusso and C. Foti, *New J. Chem.*, 2021, **45**, 20352–20364.
3 G. Aldini, B. de Courten, L. Regazzoni, E. Gilardoni, G. Ferrario, G. Baron, A. Altomare, A. D'Amato, G. Vistoli and M. Carini, *Free Radical Res.*, 2021, **55**, 321–330.
4 K. Chmielewska, K. Dzierzbicka, I. Inkielewicz-Stepniak and M. Przybyłowska, *Chem. Res. Toxicol.*, 2020, **XXXX**, A–R.
5 C. Abate, D. Aiello, M. Cordaro, O. Giuffrè, A. Napoli and C. Foti, *J. Mol. Liq.*, 2022, **368**, 120772.
6 G. Caruso, *Molecules*, 2022, **27**, 1–14.
7 G. Caruso, J. Godos, S. Castellano, A. Micek, P. Murabito, F. Galvano, R. Ferri, G. Grosso and F. Caraci, *Biomedicines*, 2021, **9**, 1–17.
8 C. Solana-Manrique, F. J. Sanz, G. Martínez-Carrión and N. Paricio, *Antioxidants*, 2022, **11**, 1–17.
9 M. Schön, A. Mousa, M. Berk, W. L. Chia, J. Ukropec, A. Majid, B. Ukropcová and B. de Courten, *Nutrients*, 2019, **11**, 1–26.
10 I. Chevalot, E. Arab-Tehrany, E. Husson and C. Gerardin, in *Industrial Biotechnology of Vitamins, Biopigments, and Antioxidants*, 2016, pp. 421–444. DOI: **10.1002/9783527681754.ch15**.
11 C. Abate, A. Scala, O. Giuffrè, A. Piperno, A. Pistone and C. Foti, *J. Environ. Manage.*, 2023, **335**, 117572.
12 M. Jozanović Horvat, M. Medvidović-Kosanović and M. Sak-Bosnar, *Int. J. Electrochem. Sci.*, 2015, **10**, 6548–6557.
13 M. Medvidovic-Kosanović, A. Stanković, M. Drulak and M. Sak-Bosnar, *Int. J. Electrochem. Sci.*, 2018, **13**, 5323–5332.
14 A. Wojnarowicz, P. S. Sharma, M. Sosnowska, W. Lisowski, T. P. Huynh, M. Pszona, P. Borowicz, F. D'Souza and W. Kutner, *J. Mater. Chem. B*, 2016, **4**, 1156–1165.
15 S. Takahashi and J.-i. Anzai, *Materials*, 2013, **6**, 5742–5762.
16 T. Moriuchi, *Eur. J. Inorg. Chem.*, 2022, **2022**, 1–10.
17 S. Martic, M. Labib, P. O. Shipman and H.-B. Kraatz, *Dalton Trans.*, 2011, **40**, 7264–7290.
18 I. R. Chowdhury, S. Chowdhury, M. A. J. Mazumder and A. Al-Ahmed, *Appl. Water Sci.*, 2022, **12**, 1–33.
19 A. Pal, S. Ranjan Bhatta and A. Thakur, *Coord. Chem. Rev.*, 2021, **431**, 1–63.
20 H. S. Mandal and H.-B. Kraatz, *J. Organomet. Chem.*, 2003, **674**, 32–37.
21 B. van der Westhuizen, J. M. Speck, M. Korb, J. Friedrich, D. I. Bezuidenhout and H. Lang, *Inorg. Chem.*, 2013, **52**, 14253–14263.

22 C. De Stefano, S. Sammartano, P. Mineo and C. Rigano, *presented in part at the Marine Chemistry: an Environmental Analytical Chemistry Approach*, 1997.
23 L. Alderighi, P. Gans, A. Ienco, D. Peters, A. Sabatini and A. Vacca, *Coord. Chem. Rev.*, 1999, **184**, 311–318.
24 P. Gans, A. Sabatini and A. Vacca, *Ann. Chim.*, 1999, **89**, 45–49.
25 I. Lavastre, J. Besançon, P. Brossiert and C. Moise, *Appl. Organomet. Chem.*, 1991, **5**, 143–149.
26 C. F. Baes and R. E. Mesmer, *The Hydrolysis of Cations*, John Wiley & Sons, New York, USA, 1976.
27 K. J. Powell, P. L. Brown, R. Byrne, T. Gajda, G. Hefter, S. Sjöberg and H. Wanner, *Pure Appl. Chem.*, 2005, **77**, 739–800.
28 K. J. Powell, P. L. Brown, R. H. Byrne, T. Gajda, G. Hefter, A.-K. Leuz, S. Sjöberg and H. Wanner, *Pure Appl. Chem.*, 2011, **83**, 1163–1214.
29 M. Filella and P. M. May, *Talanta*, 2005, **65**, 1221–1225.
30 D. Chillè, C. Foti and O. Giuffrè, *Chemosphere*, 2018, **190**, 72–79.
31 D. Chillè, D. Aiello, G. I. Grasso, O. Giuffrè, A. Napoli, C. Sgarlata and C. Foti, *J. Environ. Sci.*, 2020, **94**, 100–110.
32 D. Chillè, C. Foti and O. Giuffrè, *J. Chem. Thermodyn.*, 2018, **121**, 65–71.
33 G. Cassone, D. Chillè, V. Mollica Nardo, O. Giuffrè, R. C. Ponterio, J. Sponer, S. Trusso, F. Saija and C. Foti, *Dalton Trans.*, 2020, **49**, 6302–6311.
34 A. Gianguzza, O. Giuffrè, D. Piazzese and S. Sammartano, *Coord. Chem. Rev.*, 2012, **256**, 222–239.
35 T. Romero, A. Caballero, A. Espinosa, A. Tárraga and P. Molina, *Dalton Trans.*, 2009, 2121–2129.
36 M. Alfonso, A. Tárraga and P. Molina, *J. Org. Chem.*, 2011, **76**, 939–947.